THE JOURNAL OF BIOLOGICAL CHEMISTRY Vol. 276, No. 44, Issue of November 2, pp. 41365–41376, 2001

Printed in U.S.A.

Characterization of the Binding Interface between the Copper Chaperone Atx1 and the First Cytosolic Domain of Ccc2 ATPase*[S]

Received for publication, May 25, 2001, and in revised form, July 25, 2001
Published, JBC Papers in Press, August 10, 2001, DOI 10.1074/jbc.M104807200

Fabio Arnesano‡, Lucia Banci‡, Ivano Bertini‡§, Francesca Cantini‡, Simone Ciofi-Baffoni‡, David L. Huffman¶, and Thomas V. O'Halloran¶‖**

From the ‡Magnetic Resonance Center CERM and Department of Chemistry, University of Florence, Via Luigi Sacconi 6, Sesto Fiorentino, Florence 50019, Italy and the Departments of ¶Chemistry and the ‖Biochemistry, Molecular Biology, and Cell Biology, Northwestern University, Evanston, Illinois 60208

The interaction of the copper chaperone Atx1 and the first cytosolic domain of Ccc2 ATPase, Ccc2a, was investigated by NMR in solution. In particular, a solution of Cu(I)-^{15}NAtx1 was titrated with apo-Ccc2a, and, vice versa, a solution of Cu(I)-^{15}NCcc2a was titrated with apo-Atx1. By following the ^{15}N and ^{1}H chemical shifts, a new species is detected in both experiments. This species is the same in both titrations and is in fast exchange with the parent species on the NMR time scale. Nuclear relaxation data are consistent with the formation of an adduct. Judging from the nuclear Overhauser effect spectroscopy patterns, the structure of Cu(I)-^{15}NCcc2a in the presence of apo-Atx1 is not significantly altered, whereas Cu(I)-^{15}NAtx1 in the presence of apo-Ccc2a experiences some changes with respect to both the apoproteins and the Cu(I)-loaded proteins. The structure of the Cu(I)-^{15}NAtx1 moiety in the adduct was obtained from 1137 nuclear Overhauser effects to a final root mean square deviation to the mean structure of 0.76 ± 0.13 Å for the backbone and 1.11 ± 0.11 Å for the heavy atoms. ^{15}N and ^{1}H chemical shifts suggest the regions of interaction that, together with independent information, allow a structural model of the adduct to be proposed. The apo form of Atx1 displays significant mobility in loops 1 and 5, the N-terminal part of helix α_1, and the C-terminal part of helix α_2 on the ms–μs time scale. These regions correspond to the metal binding site. Such mobility is largely reduced in the free Cu(I)-Atx1 and in the adduct with apo-Ccc2a. The analogous mobility of Ccc2a in both Cu(I) and apo forms is reduced with respect to Atx1. Such an adduct is relevant as a structural and kinetic model for copper transfer from Atx1 to Ccc2a in physiological conditions.

Copper is an essential cofactor in hydrolytic, electron transfer, and oxygen utilization enzymes and is also crucial for high affinity uptake of iron in yeast (1, 2). Copper uptake in eukaryotes is mediated by the CTR plasma membrane proteins (3–6). Once inside the cell, a portion of the copper is delivered to P-type ATPases, which pump this metal ion into vesicles for ultimate incorporation into multicopper oxidases. In yeast, the P-type ATPase is Ccc2 (7–9), and the multicopper oxidase is Fet3 (10). The Atx1 metallochaperone protein, a cytosolic Cu(I) receptor, is required downstream of CTR1 and upstream of Ccc2 and related ATPases (11, 12). Copper chaperone proteins are soluble, intracellular receptors that bind and deliver copper to specific partner proteins (12).

Copper-trafficking pathway proteins, including homologues of CTR1 (5), Atx1 (13), Ccc2 (14–17), and Fet3 (2, 18), are highly conserved from yeast to humans. Complementation studies demonstrate that human Atx1 (Hah1) functions in place of yeast Atx1 (19), and the Wilson's and Menkes' disease proteins, homologues of Ccc2, function in place of Ccc2 to deliver copper to ceruloplasmin, a homologue of Fet3, and possibly to other proteins (20–22).

Solution structures of the native Cu(I)-bound and the reduced apo forms of both yeast Atx1 (72 amino acids) (23) and the first soluble domain of Ccc2 (Ccc2a hereafter) (72 amino acids) (24) have been recently solved. The NMR structure of the fourth domain of the Menkes transporter (25), containing an Ag(I) ion, and the crystal structure of the oxidized apo and Hg(II) forms of Atx1 (26) are also available. All of these structures share a classical "ferredoxin-like" β_1-α_1-β_2-β_3-α_2-β_4 folding (27), where the secondary structure elements, four β-strands and two α-helices, are connected by loop regions. Structural studies of Atx1 indicate that the metal-binding motif M*X*C*XX*C is located in a surface-exposed loop, with the two cysteines located in the first loop and the beginning of the first α-helix (23, 26). It has been shown that Cu(I)-Atx1 can donate its metal ion cargo to the first N-terminal Atx1-like domain of Ccc2 in a direct and reversible manner (28). Thermodynamic and kinetic considerations suggest that copper-trafficking proteins overcome the extraordinary copper chelation capacity of the eukaryotic cytoplasm by catalyzing the rate of copper transfer between physiological partners. In this sense, metallochaperones work like enzymes, carefully tailoring energetic barriers along specific reaction pathways but not others. The thermodynamic gradient for metal transfer is shallow, establishing

* This work was supported by European Community Contract HPRI-CT-1999-00009, by Italian Consiglio Nazionale delle Ricerche Contract 98.01789.CT03, and by MURST-ex 40%. The costs of publication of this article were defrayed in part by the payment of page charges. This article must therefore be hereby marked "*advertisement*" in accordance with 18 U.S.C. Section 1734 solely to indicate this fact.

[S] The on-line version of this article (available at http://www.jbc.org) contains additional figures and tabular material: one table reporting the experimental NOE intensities used for the structure calculations of Cu(I)-^{15}NAtx1 in the presence of apo-Ccc2a; four figures (Figs. 1–4) depicting the ^{15}N relaxation parameters, R_2, R_1 and ^{1}H-^{15}N NOEs for both Cu(I)- and apo-Atx1 and Cu(I)- and apo-Ccc2a; one figure (Fig. 5) reporting order parameters (S^2) of the backbone nitrogens for apoAtx1, Cu(I)- Ccc2a and apo-Ccc2a; one figure (Fig. 6) depicting ^{15}N R_1 and R_2 of the backbone nitrogens of Cu(I)-Atx1 in the presence of Ccc2a; two figures (Figs. 7 and 8 reporting the RMSD per residue to the mean structure and the number of meaningful NOE per residue for Cu(I)-^{15}NAtx1 in the presence of apo-Ccc2a; and one figure reporting the ^{15}N HSQC spectrum of Cu(I)-Atx1 in the presence of bovine serum albumin (1:1 ratio).

§ To whom correspondence may be addressed. Tel.: 39-055-4574272; Fax: 39-055-4574271; E-mail: bertini@cerm.unifi.it.

** To whom correspondence may be addressed: Dept. of Chemistry, Northwestern University, 2145 Sheridan Rd., Evanston, IL 60208. Tel.: 847-491-5060; Fax: 847-491-7713; E-mail: t-ohalloran@northwestern.edu.

that vectorial delivery of copper by Cu(I)-Atx1 is not based on a higher copper affinity of the target domain. Instead, Atx1 partner recognition allows rapid metal transfer and also protects Cu(I) from nonspecific reactions (12, 28).

Mechanistically, it has been proposed that a low activation barrier for transfer between partners results from complementary electrostatic forces that ultimately orient the metal-binding loops of Atx1 and Ccc2a for formation of copper-bridged intermediates (28). Atx1 possesses multiple positively charged lysines on its surface (23, 26), while Ccc2a possesses multiple negatively charged surface residues (24). Mutation of conserved lysines on the surface of Atx1 greatly reduces the copper-dependent interaction of Atx1 and Ccc2 *in vivo* (29). In particular, mutation of Lys^{65} of Atx1 to glutamate abrogates the function of this protein (29), thus highlighting its important role in metallochaperone function. In contrast, Ccc2a contains a phenylalanine residue at this position (24). In addition to electrostatic interactions between the two proteins, it also may be that the binding interface is templated by hydrogen bonding and hydrophobic interactions via juxtaposition of complementary surfaces.

The x-ray structures of human Atx1 (Hah1) in the presence of Cu(I), Hg(II), and Cd(II) have been recently determined (30). In contrast with yeast Hg(II)-Atx1, which crystallizes as monomer and contains Hg(II) ion with a linear coordination geometry, Hah1 crystallizes as a homodimer. The structure of Cu(I)-Hah1 reveals a copper ion coordinated by cysteine residues from two adjacent Hah1 molecules in a distorted tetrahedral array, with the fourth ligand weakly bound. This result provides structural support for direct metal ion exchange between conserved M*X*C*XX*C motifs in two domains. Moreover, the structures of Hah1 (30) provide support for three-coordinate intermediates proposed for the metal ion transfer mechanism (12).

The solution structures of Cu(I)-Atx1, apo-Atx1, Cu(I)-Ccc2a, and apo-Ccc2a provide insight into the important differences between the apo and Cu(I)-loaded forms of the proteins. Comparison of the Cu(I) and apo conformations of Atx1 reveals that the Cu(I) binding cysteines move from a buried site in the bound metal form to a solvent-exposed conformation on the surface of the protein after copper release (23). While the structure of Atx1 undergoes changes as a function of copper capture and release, the Ccc2a structure remains relatively invariant, suggesting that the metal site in apo-Ccc2a is more preorganized than in apo-Atx1 (24).

In the present work, we have characterized the interaction of Atx1 with Ccc2a. The interaction was investigated through ^1H and ^{15}N chemical shift perturbation experiments, alternately labeling the two proteins and titrating with increasing amounts of unlabeled partner. A mapping of surface residues involved in protein-protein recognition and interaction is provided together with structural models of the two proteins in the adduct. Mobility studies point out differential dynamic behavior of Atx1 and Ccc2a as a function of copper capture and release. Relaxation measurements performed on the mixture support complex formation. The results suggest a more detailed mechanism for copper exchange between the chaperone protein Atx1 and its physiological partner Ccc2. Complex formation and dissociation is rapid on the NMR time scale with a half-life for the complex on the order of milliseconds.

EXPERIMENTAL PROCEDURES

Sample Isolation and Preparation—Isotopic labeling and protein purification was performed as previously described (23, 24, 28). Protein concentrations were determined by the Bradford assay (31) and the 5,5′-dithiobis(2-nitrobenzoic acid) assay (32) and calibrated as described previously (28). Copper concentration was determined by Inductively Coupled Plasma-Atomic Emission Spectroscopy. Cu(I)-^{15}NAtx1 and Cu(I)-^{15}NCcc2a were prepared as described for the unlabeled proteins (28) and exchanged by ultrafiltration into 100 mM sodium phosphate, pH 7, 90% H_2O, 10% D_2O. The final concentration of the Cu(I)-^{15}NAtx1 NMR sample was 1.0 mM with a metal/protein ratio of 0.8:1.0. The final NMR sample concentration for Cu(I)-^{15}NCcc2a was 0.8 mM, with a metal/protein ratio of 1.3:1.0. All NMR samples were prepared under a nitrogen atmosphere at 12 °C in a VacAtmospheres chamber, where they were loaded into 535-PP 5-mm quartz NMR tubes (Wilmad) and sealed with latex serum caps.

NMR Titration of the Two Proteins—Titrations of Cu(I)-^{15}NAtx1 with unlabeled apo-Ccc2a and of Cu(I)-^{15}NCcc2a with unlabeled apo-Atx1 were performed with NMR spectroscopy, following the ^{15}N-^1H spectral changes upon the addition of increasing amounts of the unlabeled proteins. Aliquots were added in a Coy chamber under nitrogen atmosphere at 298 K using a Hamilton syringe to deliver small amounts of unlabeled proteins to the labeled samples in NMR tubes. The starting Cu(I)-^{15}NAtx1 and Cu(I)-^{15}NCcc2a samples were 1.0 and 0.8 mM in concentration, respectively. The additions ranged from 0.05 to 0.9 mM in apo-Ccc2a and from 0.1 to 0.7 mM in apo-Atx1. The final labeled protein concentration was 0.7 mM for Cu(I)-^{15}NAtx1 and 0.5 mM for Cu(I)-^{15}NCcc2a.

NMR Spectroscopy—All of the NMR spectra except for ^1H-^{15}N NOE,[1] R_1, and R_2 relaxation experiments, were acquired on a Ultra Shield 700 Bruker spectrometer operating at proton nominal frequency of 700.13 MHz. A triple resonance 5-mm probe was used.

All two-dimensional ^{15}N HSQC (33–35) spectra were recorded with an INEPT delay of 2.5 ms, a recycle time of 1 s, and spectral windows of 14 and 33 ppm for the ^1H and ^{15}N dimensions, respectively. Two-dimensional TOCSY (36, 37) and NOESY (38), and three-dimensional NOESY-^{15}N HSQC (39) experiments were recorded on Cu(I)-^{15}NAtx1/apo-Ccc2a samples with protein concentration ratios of 1:0.5 and 1:1. The same spectra were also recorded on Cu(I)-^{15}NCcc2a/apo-Atx1 mixtures with protein ratios of 1:0.4 and 1:1.

The two-dimensional NOESY experiments were acquired with a mixing time of 100 ms, a recycle time of 1 s, and a spectral window of 14 ppm. The TOCSY spectra were recorded with a spin lock time of 100 ms, a recycle time of 1 s, and a spectral window of 14 ppm.

The three-dimensional NOESY-^{15}N HSQC experiments were recorded with 160 (^1H) $\times$ 88 (^{15}N) $\times$ 1024 (^1H) data points. In these experiments, the INEPT delay was set to 2.5 ms, the mixing time was 100 ms, and the carrier frequency was set at the center of the amide proton region, at 8.0 ppm. Spectral windows of 14, 14, and 33 ppm were used for the direct ^1H dimension and the indirect ^1H and ^{15}N dimensions.

Relaxation experiments were collected on Bruker Avance 500 and 400 spectrometers, operating at proton nominal frequencies of 500.13 and 400.13 MHz, respectively. Relaxation experiments on Cu(I)-^{15}NAtx1 were carried out at 500 MHz. Relaxation experiments on apo-^{15}NAtx1, on Cu(I)-^{15}NAtx1 in the presence of apo-Ccc2a (final step of the titration at 1:1.25, Cu(I)-^{15}NAtx1/apo-Ccc2a ratio), and on ^{15}NCcc2a, in the apo and copper-bound forms, were carried out at 400 MHz. A triple resonance 5-mm probe was used with an Avance 500-MHz spectrometer, and a broad band observing probe for direct detection of the X nucleus was used with an Avance 400-MHz spectrometer. All of the probes were equipped with pulsed field gradients along the *z* axis.

The ^{15}N backbone longitudinal relaxation rates, R_1, were measured as previously described (40) using delays in the pulse sequence of 5, 35, 75, 125, 190, 270, 370, 500, 675, 1000, and 1750 ms for all samples. The ^{15}N backbone transverse relaxation rates, R_2, were measured using the CPMG sequence as described elsewhere using a refocusing delay (τ_{CPMG}) of 450 μs (40). To monitor the changes of the transverse relaxation rates in the presence of relatively weak effective fields, R_2 rates were also measured as a function of the τ_{CPMG} value (40, 41). Experiments were collected at six CPMG refocusing delays τ_{CPMG}: 450, 550, 700, 850, 1000, and 1150 μs. Relaxation delays varied from 7 to 230 ms, the exact values depending on τ_{CPMG}. In the R_1 and R_2 measurements, eight scans were collected for each experiment. The heteronuclear ^1H-^{15}N NOE were measured using the pulse scheme published by Grzesiek

[1] The abbreviations used are: NOE, nuclear Overhauser effect; INEPT, insensitive nuclei enhanced by polarization transfer; HSQC, heteronuclear single quantum coherence; NOESY, nuclear Overhauser effect spectroscopy; TOCSY, total correlation spectroscopy; R_1, longitudinal relaxation rate; R_2, transverse relaxation rate; CPMG, Carr-Purcell-Meiboom-Gill; WATERGATE, water suppression by gradient-tailored excitation; r.m.s., root mean square.

and Bax (42) and considering the ratio of the peak volumes in spectra recorded with and without ^{1}H saturation.

For all experiments, quadrature detection in the indirect dimensions was performed in the time-proportional phase incrementation mode (43), and water suppression was achieved through WATERGATE sequence (44), except the heteronuclear ^{1}H-^{15}N NOE experiments, where the pulse sequence applies *flip back* pulses for water suppression. All two-dimensional NOESY and TOCSY spectra consisted of 4096 data points in the acquisition dimension and of 1024 experiments in the indirect dimension. R_1, R_2, and ^{1}H-^{15}N NOE two-dimensional spectra consisted of 2048 data points in the acquisition dimension and of 256 experiments in the indirect dimension.

All of the spectra were collected at 298 K, processed using the standard Bruker software (XWINNMR), and analyzed on IBM RISC 6000 computers through the XEASY program (45). Integration of cross peaks in the R_1, R_2, and ^{1}H-^{15}N NOE measurements was performed by using the standard routine of the XWINNMR program.

Relaxation Data Analysis—Relaxation rates R_1 and R_2 were determined by fitting the cross-peak intensities (I), measured as a function of the delay (T) within the pulse sequence, to a single exponential decay by using the Levenburg-Marquardt algorithm (46, 47) according to the following equation,

$$I(T) = A + B \cdot \exp(-RT) \qquad \text{(Eq. 1)}$$

where A, B, and R were adjustable fitting parameters. For R_2, the phase cycle was chosen so that the magnetization relaxes to 0 for long relaxation delays; thus, in this case, A was set equal to 0 in the fitting procedure. A program that uses a Monte Carlo approach to estimate the error on the rates (48–50) was used.

The experimental longitudinal and transverse relaxation rates and the heteronuclear NOEs have been analyzed with the Model-Free 4.0 program (51), within the Lipari-Szabo approach (52). This program models overall rotational diffusion using a diffusion tensor, D. R_1, R_2, and NOE values for ^{15}N spins are determined by the dipolar coupling with the attached proton and, for R_1 and R_2, also by the chemical shift anisotropy of the nitrogen spins. The equations for these rates, in terms of spectral density functions ($J(\omega)$), are reported in the literature (53). Within the Model-Free approach (48, 51) the spectral density functions $J(\omega)$ can be expressed as a function of the overall rotational correlation time, τ_m, of the order parameter S^2 and of the correlation time for internal motions, which can be considered as arising from two components, one describing faster (τ_f) and one slower (τ_s) motions (collectively called τ_e), but always faster than τ_m.

Having available the three-dimensional structures of Atx1 (23) and Ccc2a (24) in both Cu(I) and apo forms, the initial τ_m values and the rotational diffusion tensor can be estimated from the R_2/R_1 ratio with the program *quadric_diffusion* (54, 55). In the present analysis, we have used an axially symmetric model to account for the global rotational motion (56–58). Once the best model for the molecular motions is selected on the basis of an F statistic test (51) of the Model-Free analysis, the overall τ_m, the ratio $D_\parallel/D_\perp$, and the internal motional parameters for each spin are optimized by fitting the experimental relaxation parameters R_1, R_2, and NOE to their equations (53). The Powell minimization algorithm (see Ref. 47) has been used.

R_2 can also contain a contribution R_{ex}, originating from exchange processes in the millisecond to microsecond time range. In the present work, we have also used an independent experimental method (^{15}N R_2-CPMG experiments (59)) to specifically probe and accurately determine the exchange processes occurring with correlation times τ_{ex} in the range between 100 and 500 μs. This allows us to take into account these processes in the analysis of R_1, R_2, and NOEs for the estimation of the values of the order parameter and the correlation time for the internal motions.

A dependence of R_2 on the length of τ_{CPMG} delay indicates an exchange contribution R_{ex} to transverse relaxation rate. The exchange contribution R_{ex} can be expressed by the following Equation 2 (60) in terms of the weak effective magnetic field, ν_{eff}, applied in the xy plane and resulting from the CPMG pulse train.

$$R_{ex} = \frac{k_{ex}}{2} - 2\nu_{eff}\, sinh^{-1}\left(\frac{k_{ex}}{\xi}\, sinh\, \frac{\xi}{4\nu_{eff}}\right) \qquad \text{(Eq. 2)}$$

where $\xi = (k_{ex}{}^2 - 4p_Ap_B\delta\omega^2)^{1/2}$ and $k_{ex} = 1/\tau_{ex}$. The effective field strength at each delay is related to the τ_{CPMG} length by the following equation,

$$\nu_{eff}(s^{-1}) = \frac{1}{2(T_{\pi} + \tau_{CPMG})} \qquad \text{(Eq. 3)}$$

where T_π is the duration of a 180° ^{15}N CPMG pulse (80 and 60 μs for the experiments collected at 500 and 400 MHz, respectively). When the τ_{ex} is longer than τ_{CPMG}, no effect due to conformational exchange processes is observed.

Experimental limits on the spin echo delay length are determined by the duty cycle of the transmitter for short delays and the evolution of ^{1}H-^{15}N coupling during long delays.

Constraints Used in Structure Calculations—The NOE dipolar connectivities, transformed in distance constraints through the program CALIBA (61) to be used for structural calculations, were integrated in the two-dimensional NOESY map acquired at 298 K in H_2O on the mixture containing a Cu(I)-^{15}NAtx1/apo-Ccc2a ratio of 1:1. The calibration curves were adjusted iteratively as the structure calculations proceeded. Stereospecific assignments of diastereotopic protons were obtained using the program GLOMSA (61).

Structure Calculations—Structure calculations on Cu(I)-^{15}NAtx1 in the complex were performed using the program DYANA (62), without inclusion of links with the copper ion. 200 random conformers were annealed in 10,000 steps using the above constraints. The 20 conformers with the lowest target function constitute the final family.

The program CORMA (63), which is based on relaxation matrix calculations, was used to back calculate the NOESY cross-peaks from the calculated structure and to check the consistency of the whole procedure. This has also allowed us to assign a few more cross-peaks between already assigned resonances.

The quality of the structure was evaluated in terms of deviations from ideal bond lengths and bond angles and through Ramachandran plots obtained using the programs PROCHECK (64) and PROCHECK-NMR (65).

Structure calculations and analysis were performed on IBM RISC 6000 computers.

RESULTS

Mobility of Cu(I) and Apo Forms of Atx1 and Ccc2a—In order to characterize the interaction between Atx1 and Ccc2a, it was necessary to study the mobility of the two proteins both with and without copper.

From the ratio R_2/R_1, an initial estimate of the τ_m was calculated for each protein. In this analysis, care was taken to remove from the input relaxation data those NHs having an exchange contribution to the R_2 value or exhibiting large amplitude internal motions in a time scale longer than a few hundred ps, identified from low NOE values, since inclusion of these data would bias the calculated rotational diffusion tensor parameters (66, 67). The values of τ_m for apo-^{15}NAtx1, Cu(I)-^{15}NCcc2a, and apo-^{15}NCcc2a are 4.4 ± 0.2, 4.6 ± 0.3, and 4.5 ± 0.3 ns, respectively. These values are consistent with the expectation from the Stokes-Einstein isotropic model (68). For Cu(I)-^{15}NAtx1, τ_m was 5.1 ± 0.2 ns. This value could indicate a slight aggregation of Atx1 molecules upon metal binding. Copper induced self-aggregation was observed, to a larger extent, in the bacterial copper transporter CopZ from *Enterococcus hirae*, having the same fold and the same metal-binding motif M*X*C*XX*C of Atx1 (69).

R_1, R_2, and heteronuclear NOE for Cu(I)-bound and apo forms of both Atx1 and Ccc2a are reported in the supplemental material (supplemental Figs. 1–4). The order parameters characterizing the internal mobility have been determined within the Lipari-Szabo model (52) for the three proteins that are completely in a monomeric form by using the Model-Free 4.0 program (51). Also, such values are reported as supplemental material (supplemental Fig. 5).

From the analysis of the data, it appears that there are no residues significantly mobile on a fast time scale, the S^2 values being homogeneous along the protein sequence for apo-^{15}NAtx1 (average S^2 value = 0.88 ± 0.04) and Ccc2a (average S^2 values are 0.85 ± 0.03 for Cu(I)-^{15}NCcc2a and 0.87 ± 0.03 for apo-^{15}NCcc2a).

The overall correlation time for molecular tumbling, τ_m and the $D_\parallel/D_\perp$ ratio for apo-^{15}NAtx1 and for Cu(I)- and apo forms of ^{15}NCcc2a were fitted during the last stage of the Model-Free

TABLE I
Backbone amide nitrogens involved in conformational exchange processes in Cu(I)- and apo-Atx1 and in the adduct at a protein ratio Cu(I)-[15]NAtx1/apoCcc2a, 1:1.25

Residue	τ_{ex}[a]		
	Cu(I)	Apo	Adduct
		μs	
5	150 ± 30		
8		150 ± 52	
13		150 ± 20	
15		140 ± 15	
19	370 ± 25	120 ± 20	
23			—[b]
24			—[b]
26		160 ± 30	
28		170 ± 30	
55		170 ± 20	
61		150 ± 50	
62		136 ± 20	—[b]
63	110 ± 50	170 ± 20	320 ± 30
64		380 ± 40	
65		370 ± 30	
70		166 ± 15	
71		160 ± 10	
72		140 ± 15	

[a] Correlation time of the exchange process, τ_{ex}, obtained by fitting data to Equation 2.
[b] —, for this residue the measured R_2 value is larger than the average and might indicate the presence of an R_{ex} contribution to the transverse relaxation rate, due to a conformational exchange process on a time scale (τ_{ex} <100 μs) faster than the range sampled by CPMG experiments.

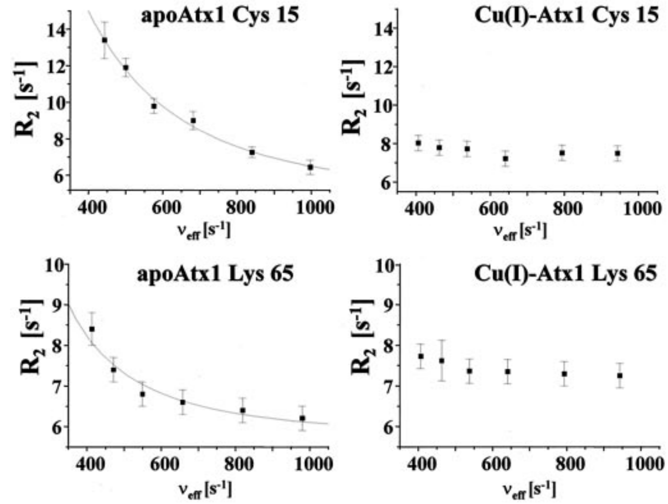

FIG. 1. **Representative fittings of the relaxation rates R_2 to Equation 2 for residues Cys[15] (loop 1) and Lys[65] (loop 5) in apo- and Cu(I)-Atx1.**

TABLE II
[15]N nuclei involved in conformational exchange processes in Cu(I)- and apo-Ccc2a

Residue	τ_{ex}[a]	
	Cu(I)	Apo
	μs	
2		170 ± 30
10		290 ± 80
12		320 ± 125
13	440 ± 40	—[b]
17		138 ± 5
19		400 ± 100
27		180 ± 30
33		150 ± 40
51		160 ± 30

[a] Correlation time of the exchange process, τ_{ex}, obtained by fitting data to Equation 2.
[b] —, [15]N backbone atom whose relaxation rate could not be measured due to low intensity of the peak.

calculations. The $D_\|/D_\perp$ ratio was found to be in the range of 1.1–1.3 for both proteins. The optimized final τ_m value is 4.58 ± 0.05 ns for apo-[15]NAtx1 and 4.60 ± 0.05 and 4.29 ± 0.04 ns for Cu(I)- and apo-[15]NCcc2a, respectively.

Within the Model-Free analysis, residues displaying conformational exchange are fitted with an R_{ex} contribution to R_2. In the present work, the presence of this contribution was independently evaluated by measuring the transverse relaxation rates, R_2, of the backbone amide nitrogens as a function of the τ_{CPMG} duration, which produces different effective field strengths, ν_{eff}, given by Equation 3. A dependence of R_2 on ν_{eff} indicates the presence of exchange phenomena that contribute to the transverse relaxation rate. In order to evaluate the exchange correlation time, τ_{ex}, the R_2 values have been fitted against ν_{eff} to Equation 2. In our experimental conditions, the τ_{ex} values of exchange between two conformational substates range between 110 and 440 μs. The analysis has been performed for the apo and the Cu(I)-bound forms of both Atx1 and Ccc2a, and exchange processes, found from Model-Free analysis, were consistently detected also through these CPMG measurements.

In Cu(I)-[15]NAtx1, only three residues show a dependence of R_2 on ν_{eff}. In apo-[15]NAtx1, this number increases to 15. These results are summarized in Table I together with the correlation time of the exchange process, τ_{ex}, obtained from the fitting to Equation 2. In Fig. 1, two representative fittings are shown for residues Cys[15] (loop 1) and Lys[65] (loop 5) in both apo- and Cu(I)-[15]NAtx1. Both residues experience a decay of R_2 with ν_{eff} in the apo form, while no decay has been detected in the copper-bound state. In apo-[15]NCcc2a and Cu(I)-[15]NCcc2a, the number of residues displaying a dependence of R_2 on ν_{eff} is eight and one, respectively, and they are reported in Table II. Residues involved in conformational exchange equilibria for the Cu(I)-bound and apo forms of Atx1 and Ccc2a are shown in Fig. 2 (*a–d*). The dynamic characterization of the two proteins identifies a different mobility in the copper binding region; the apo form of Atx1 shows more conformational exchange processes than apo-Ccc2a, and the copper binding to Atx1 makes the metal binding region more rigid. In particular, loop 5 and the C-terminal part of helix α_2, both adjacent to the metal site, display conformational exchange processes in apo-Atx1 but not in apo-Ccc2a. This result is consistent with the fact that, relative to Atx1 (23), copper binding induces fewer changes in the conformation of Ccc2a (24).

Titration of Cu(I)-[15]NAtx1 with Unlabeled Apo-Ccc2a and of Cu(I)-[15]NCcc2a with Unlabeled Apo-Atx1—Two-dimensional [15]N-[1]H HSQC spectra were recorded at 700 MHz on Cu(I)-[15]NAtx1 and Cu(I)-[15]NCcc2a samples. By previous convention, the first amino acid in Atx1 is denoted as Ala[2] and the last as Leu[73]. The N-terminal Met of Atx1 is processed in *Escherichia coli*, yielding a 72-amino acid protein (23). The HSQC map of Cu(I)-[15]NAtx1 showed the presence of only one form, the same as that already reported as form A (23). In previous preparations, a minor form B was also present (23). Cross-peaks of amide protons of residues 2, 3, and 16 were not present. For the apo form, amide resonances were missing for residues 2–3, 14, and 16–18 at 298 K. Each cross-peak corresponds to an NH moiety, and a missing cross-peak may mean exchangeability of the amide proton with bulk water. In the [15]N-[1]H HSQC spectrum of Cu(I)-[15]NCcc2a, the NH cross-peaks for residues 1 and 14 were not present. Furthermore, as previously reported (24), peaks of residues 10 and 12 were broadened in apo-[15]NCcc2a with respect to the copper-bound form, and the cross-peaks of residues 1, 14, and 15 were missing.

Cu(I)-[15]NAtx1 and Cu(I)-[15]NCcc2a were then titrated with

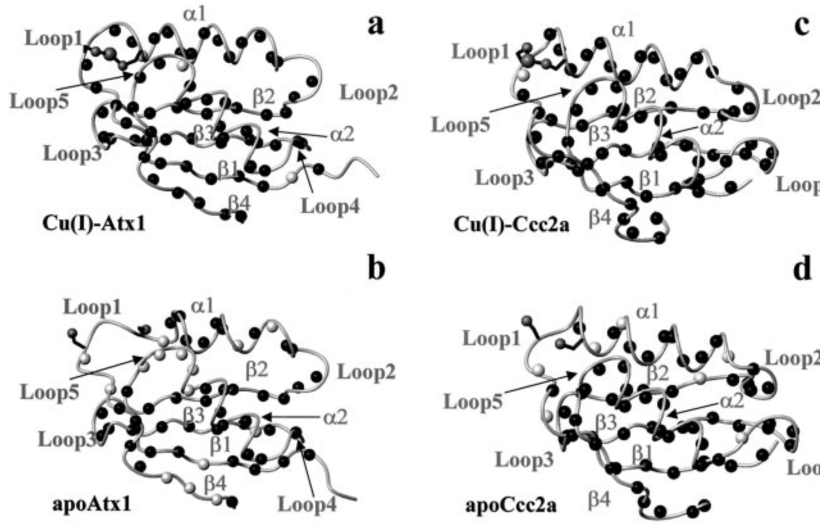

FIG. 2. **Mapping of ^{15}N mobility in the millisecond to microsecond time scale in the protein frame of Cu(I)-Atx1 (*a*), apo-Atx1 (*b*), Cu(I)-Ccc2a (*c*), and apo-Ccc2a (*d*).** *Black spheres* indicate ^{15}N atoms of residues for which no dependence of the R_2 on ω_{eff} was detected. *White spheres* indicate ^{15}N atoms of residues experiencing exchange processes.

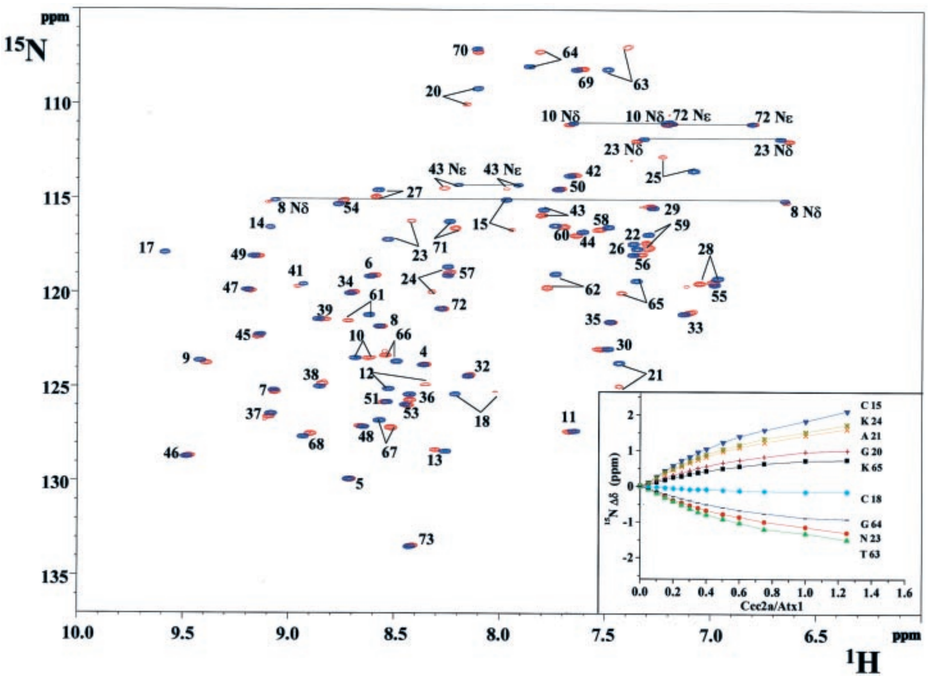

FIG. 3. **Superposition of two-dimensional ^{15}N-^{1}H HSQC spectra (700 MHz, 298 K) of uncomplexed Cu(I)-^{15}NAtx1 (*blue*) and of the Cu(I)-^{15}NAtx1·apo-Ccc2a complex (*red*) at a ratio of 1:1.** The *inset* shows backbone amide chemical shifts as a function of apo-Ccc2a concentration for some Atx1 residues exhibiting measurable changes.

unlabeled apo-Ccc2a and apo-Atx1, respectively. Spectral changes were measured by ^{15}N-^{1}H HSQC experiments. In both titrations, the ^{1}H and ^{15}N resonances showed changes in shift with increasing amounts of unlabeled apo-Ccc2a and apo-Atx1. Furthermore, a few residues experience some broadening. Such spectral changes indicate that (i) Ccc2a is interacting with Atx1 and (ii) the exchange rate between free and "interacting" species is larger than the difference in chemical shift, indicating that the proteins in the complex are in fast exchange with the free proteins in solution.

The spectral changes were followed up to a final apo-Ccc2a concentration of 0.9 mM with a final Cu(I)-^{15}NAtx1 concentration of 0.7 mM and an apo-Atx1 concentration of 0.7 mM with a final Cu(I)-^{15}NCcc2a concentration of 0.5 mM. Fig. 3 shows the ^{15}N-^{1}H HSQC of the Cu(I)-^{15}NAtx1 protein (*blue contours*) overlaid onto that of the Cu(I)-^{15}NAtx1/apo-Ccc2a mixture containing equal concentrations of the two proteins (*red contours*). Cross-peaks of Cu(I)-^{15}NAtx1 residues Thr^{14} and Gly^{17} broadened beyond detection. These residues are close to the Atx1 copper ligands (Cys^{15} and Cys^{18}), and they might experience the largest change in shift between the isolated and the mixture states. If the exchange rate between the free form and the adduct with Ccc2a is equal to or larger than the chemical shift difference, then signal broadening and even signal coalescence can occur. Twenty-six backbone NHs (10, 12–13, 15, 18–28, 36, 43, 59, 61–67, and 71) and the $N_{\epsilon}H_2$ of Gln^{43} maintained narrow line widths and had measurable shift changes throughout the titration.[2]

In the ^{15}N-^{1}H HSQC spectra of Cu(I)-^{15}NCcc2a collected at increasing concentrations of apo-Atx1, the cross-peaks of residues 8–11, 13, 15–24, 26, 29–30, 55, 57–59, and 62–67 exhibited measurable changes in the chemical shifts. Moreover, the cross-peaks of residues 12 and 15 broadened and eventually disappeared during the titration, while cross-peaks of residues 9, 13, 19, 21, 23, and 64 broadened significantly. The cross-peak of one of the protons of $N_{\epsilon}H_2$ of Gln^{23} shifted significantly, whereas the other proton cross-peak was invariant. This might

[2] The specificity of the spectral changes was checked through a control experiment where Cu(I)-^{15}NAtx1 was titrated with bovine serum albumin. No shift change, both in the ^{1}H and ^{15}N dimensions, has been detected up to a protein/protein ratio of 1:1.

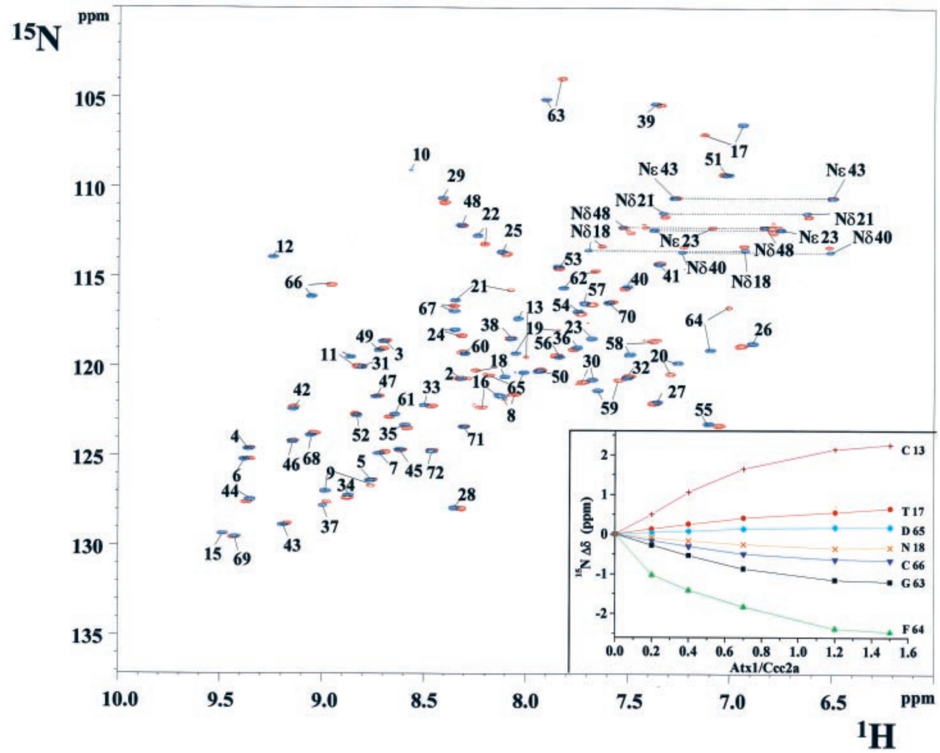

FIG. 4. **Superposition of the two-dimensional ^{15}N-^{1}H HSQC spectra (700 MHz, 298 K) of uncomplexed Cu(I)-^{15}NCcc2a (*blue*) and the Cu(I)-^{15}NCcc2a·apo-Atx1 complex (*red*) at a ratio of 1:1.** The *inset* shows backbone amide chemical shifts as a function of apo-Atx1 concentration for some Ccc2a residues exhibiting measurable changes.

suggest the formation of a hydrogen bond between Gln^{23} and Atx1. Fig. 4 shows the ^{15}N-^{1}H HSQC of the Cu(I)-^{15}NCcc2a protein (*blue contours*) overlaid onto that in the presence of apo-Atx1 in 1:1 ratio (*red contours*).

The midpoint of the spectral changes occurred at 0.35–0.40 mM concentration of the titrant for both titrations (*insets* of Figs. 3 and 4). This indicates that the two association processes occur with a similar dissociation constant. By fitting the titration data to a simple three-component model (70) in which Atx1 combines with Ccc2a to a complex (intermediate), we can estimate a K_d of $\sim 10^{-3}$ to 10^{-4} M for both titrations.

Analysis of three-dimensional NOESY-^{15}N HSQC and two-dimensional NOESY and TOCSY maps of the final mixtures was used to confirm and extend the assignment of ^{15}N-^{1}H HSQC spectra. The TOCSY map was used to identify spin patterns of intraresidue connectivities of the different amino acids. Then these residues were connected to other spin patterns by sequential characteristic NOESY peaks. The three-dimensional map was used to solve problems of cross-peak overlap in the two-dimensional NOESY map and to confirm the assignment of the ^{15}N resonances.

The ^{1}H and ^{15}N chemical shift differences between Cu(I)-^{15}NAtx1 alone and in the 1:1 mixture are reported on the *left side* of Fig. 5. The weighted average chemical shift differences Δ_{avg}(HN) shown in the *lower plots* of Fig. 5 were calculated as described by Garrett *et al.* (71) (*i.e.* $((\Delta H)^2 + (\Delta N/5)^2)/2)^{1/2}$, where ΔH and ΔN are chemical shift differences for ^{1}H and ^{15}N, respectively). For the purpose of comparison, differences in chemical shifts between Cu(I)-^{15}NAtx1 and its apo form (23) are also shown in Fig. 5 on the *right*. It can be seen clearly that the major changes in the Cu(I)-^{15}NAtx1 signals caused by the addition of apo-Ccc2a are localized in two regions of the protein corresponding to stretches 10–30 and 60–70. These stretches constitute loop 1, helices α_1 and α_2, and loop 5. Chemical shift differences between Cu(I)- and apo-^{15}NAtx1 were also found in these regions, but the pattern is different from that determined by the presence of apo-Ccc2a. Differences in the stretch 60–70 are here smaller than in the presence of apo-Ccc2a.

The differences in chemical shifts between Cu(I)-^{15}NCcc2a alone and in the 1:1 mixture are reported on the *left* of Fig. 6. Differences between Cu(I)-^{15}NCcc2a and its apo form are also shown. As for Cu(I)-^{15}NAtx1, the major changes in the Cu(I)-^{15}NCcc2a signals caused by the addition of apo-Atx1 are localized in two regions of the protein corresponding to stretches 8–23 and 55–66 that form loop 1, the first segment of helix α_1, the last segment of helix α_2, and loop 5. Chemical shift differences between Cu(I)- and apo-^{15}NCcc2a were found only in the region 12–21 (loop 1 and helix α_1). Therefore, changes in chemical shift between Cu(I)-^{15}NCcc2a and its apo form, obtained for pure samples of each protein, are different from those determined by the presence of apo-Atx1.

The question then arises of whether the final adduct is the same regardless of which protein carries copper. This was addressed through the analysis of the ^{1}H two-dimensional NOESY spectra of the mixtures, Cu(I)-^{15}NAtx1/apo-Ccc2a (unlabeled) and Cu(I)-^{15}NCcc2a/apo-Atx1 (unlabeled). By following the shifts affected by the formation of the adduct for protons of the other, unlabeled protein, it appears that the extrapolated final spectrum is the same. Therefore, either the final species is the same, or there is the same average of species in fast exchange.

Structural and Dynamic Characterization of the Adduct of Cu(I)-^{15}NAtx1 with apo-Ccc2—R_2 and R_1 experiments, performed on the Cu(I)-^{15}NAtx1/apo-Ccc2 mixture in the final step of the titration, showed that, overall, the transverse relaxation rates are increased with respect to pure Cu(I)-^{15}NAtx1. For Cu(I)-^{15}NAtx1 in the mixture, τ_m was estimated using the R_2/R_1 ratio and found to be 8.5 $\pm$ 0.7 ns. This value is consistent with about 70% formation of protein-protein adduct, assuming a double overall rotational correlation time for molecular tumbling of the complex, due to a roughly double molecular mass (8088 (Atx1) + 7882 (Ccc2a) Da from mass spectra). The picture of adduct formation is consistent with that coming out from the titration.

Transverse relaxation rates, measured with a spin echo delay τ_{CPMG} = 450 μs on ^{15}N Cu(I)-^{15}NAtx1/apo-Ccc2 mixture,

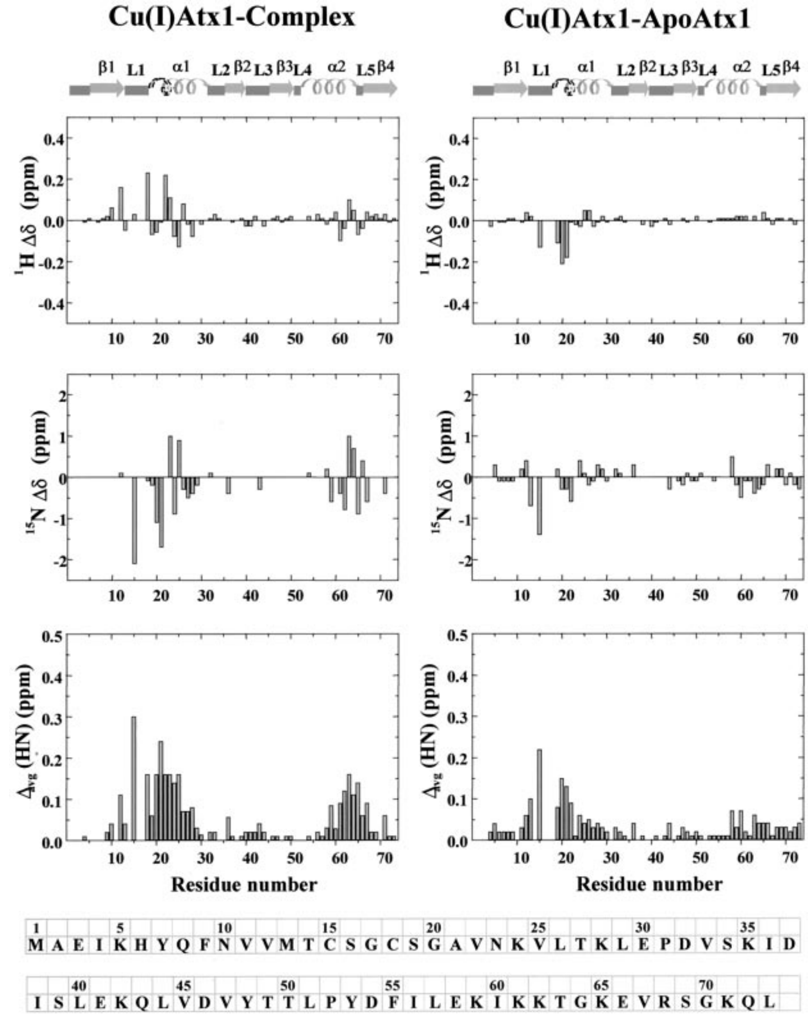

FIG. 5. **^{1}H and ^{15}N amide chemical shift differences between pure Cu(I)-^{15}NAtx1 and the 1:1, Cu(I)-^{15}NAtx1/apo-Ccc2a mixture (*left side*).** The weighted average chemical shift differences Δ_{avg}(HN) (see "Results") are shown in the *bottom plot*. Differences in chemical shifts between Cu(I)-^{15}NAtx1 and its apo form are also shown (*right side*). Chemical shift differences are not reported for residues 2–3, 14, and 16–17, since their ^{1}H-^{15}N cross-peaks are not observed in the presence of apo-Ccc2a. In addition, the cross-peak of residue 18 is not observed in apo-^{15}NAtx1. The secondary structure elements of Cu(I)-Atx1 are reported at the *top*. The first turn of helix α_1 (*dashed*) is not formed in the apo structure. The sequence of yeast Atx1 is reported at the *bottom*.

are fairly homogeneous over the protein sequence (10.1 ± 0.9 Hz on average). Residues 23, 24, 62, and 63 show R_2 values slightly higher than the average (see Fig. 6 of supplemental material). CPMG measurements indicate a conformational exchange process in the millisecond to microsecond time scale only for residue Thr^{63}. Therefore, Cu(I)-^{15}NAtx1 in the adduct shows a more rigid metal site with respect to its apo form but similar to the copper-bound form (see Table I).

The structure of Cu(I)-^{15}NAtx1 in the presence of apo-Ccc2a was calculated using experimental distance constraints obtained from NOESY maps. In total, 2320 NOESY cross-peaks were assigned and integrated. They were transformed into upper distance limits with the program CALIBA (61) and resulted in 1470 unique upper distance limits, of which 1137 were meaningful.[3] A total of 49 proton pairs were stereospecifically assigned through the program GLOMSA (61). The NOEs and the r.m.s. deviation per residue are reported as supplementary material.

The 20 conformers constituting the final DYANA family have an average target function of 1.1 ± 0.12 Å^2 and an average r.m.s. deviation to the mean structure (for residues 4–73) of 0.76 ± 0.13 Å for the backbone and 1.11 ± 0.11 Å for the heavy atoms. The resolution is quite good, especially if it is considered that some amino acids are not detected.

The family of conformers was analyzed with PROCHECK-NMR (65). 94% of residues fall in the core and allowed regions of the Ramachandran plot. 5% of residues are in the generously allowed region, and 1% are in the disallowed region.

The largest backbone r.m.s. deviation values are obtained for residues at the N terminus and for the region 14–21, containing loop 1 and the beginning of helix α_1 (the average backbone r.m.s. deviation value for residues 14–21 is 1.3 ± 0.3 Å). However, the rest of the protein is well defined. As mentioned above, amide peaks of residues 14 and 17 in the Cu(I)-^{15}NAtx1/apo-Ccc2 mixture are not detectable due to signal broadening. Previous studies revealed that region 14–21 was also less defined in apo-Atx1 (23). The resulting structure, especially for the conformationally labile part of loop 1, is a time average structure of different conformers.

The NOE pattern for Cu(I)-^{15}NCcc2a is the same independent of the adduct formation. Therefore, it is concluded that the polypeptide chain of Ccc2a has the same fold and conformation in the adduct as in the apo and in the Cu(I)-loaded forms (24).

DISCUSSION

Interaction between the Two Proteins—During the titrations of Cu(I)-^{15}NAtx1 with apo-Ccc2a and of Cu(I)-^{15}NCcc2a with apo-Atx1, changes observed in the HSQC spectra can arise from perturbations due either to protein-protein interactions or copper transfer or both.

In the present titrations, a single signal was detected for each nucleus, with the shift changing with the concentration of the other protein. The behavior indicates a fast exchange between the free states and a complex. The NH chemical shift

[3] Nonmeaningful distance constraints are those that cannot be violated in any structure conformation and those involving proton pairs at fixed distance.

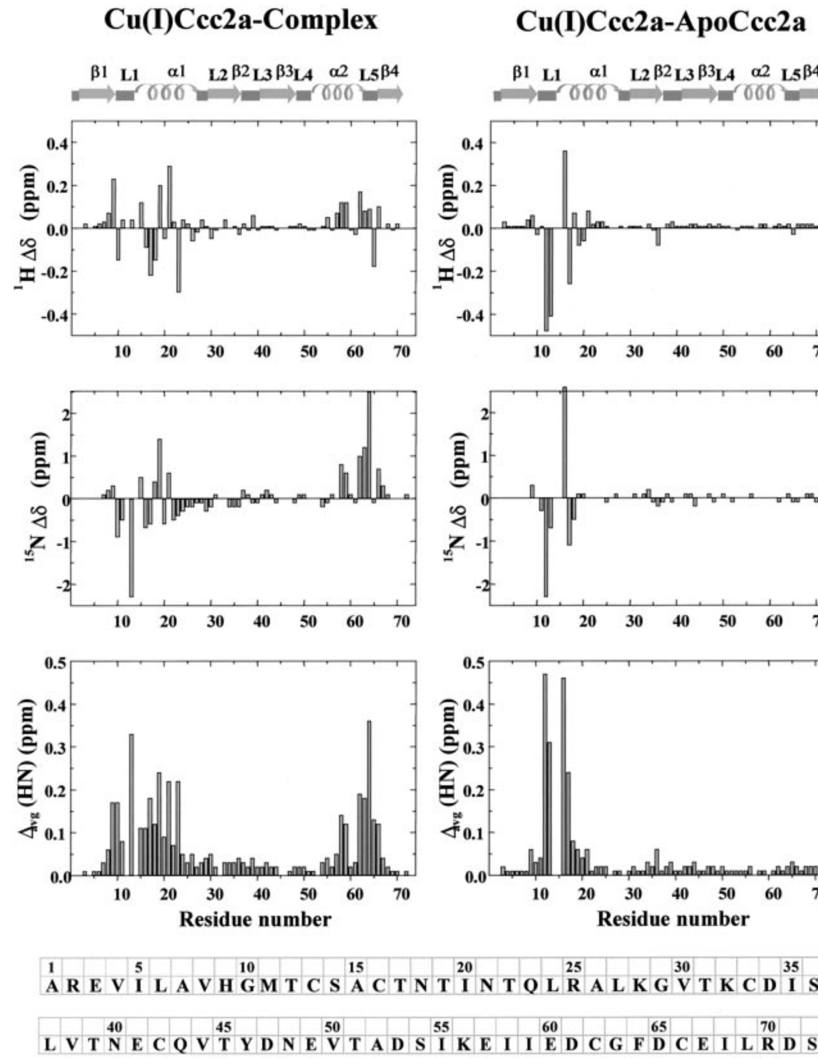

FIG. 6. **^{1}H and ^{15}N amide chemical shift differences between pure Cu(I)-^{15}NCcc2a and the 1:1 Cu(I)-^{15}NCcc2a/apo-Atx1 mixture (*left side*).** The weighted average chemical shift differences Δ_{avg}(HN) are shown in the *bottom plot*. These differences are not reported for residues 1, 12, and 14, since their ^{1}H-^{15}N cross-peaks are not observed in the presence of apo-Atx1. Differences in chemical shifts between Cu(I)-^{15}NCcc2a and its apo form are also shown (*right side*). In apo-^{15}NCcc2a, cross-peaks of residues 1, 14, and 15 are not observed. The secondary structure elements of Cu(I)-Ccc2a are reported at the *top*. The sequence of yeast Ccc2a is reported at the *bottom*.

changes between the free and the complexed forms of both Cu(I) proteins were different from those observed in the corresponding apo forms (see Figs. 5 and 6). The ~70% increase in the overall correlation time for molecular tumbling of the new species suggests strongly that the two proteins were interacting in solution and forming a protein-protein complex.

Line broadening observed for some resonances during the titrations can be due either to a chemical shift difference close to the exchange rate between the free and bound form or to an increased local mobility of specific residues in the adduct. In particular, after the addition of the partner, the NH signals of Thr^{14} and Gly^{17} in Cu(I)-^{15}NAtx1 and Thr^{12} and Ala^{15} in Cu(I)-^{15}NCcc2a broadened beyond detection, suggesting that they are perturbed significantly by protein-protein interactions. Interestingly, these resonances are readily assigned in the Cu(I) forms but are broadened or not detected in apo forms of either protein. Furthermore, in both proteins, these residues occupy corresponding positions in the metal-binding motif, *i.e.* before the first and the second Cys, respectively.

The chemical shift differences between the original and new resonances observed in both titrations, allow estimation of a lower limit for the rate constant k_D for dissociation of the complex. The maximum observed shift change without significant line broadening is ~200 Hz (for the ^{1}HNϵ proton of the side chain amide of Gln^{23} of Ccc2a) yielding a lower limit of ~1250 s^{-1} for k_D (70). Since a saturation point was not obtained during the titration, the lower limit is actually greater than this. Assuming a bimolecular second order process and realizing that the forward rate constant cannot be faster than the diffusion-controlled limit (10^8 to 10^9 M^{-1} s^{-1}), we estimate that K_d is ~10^{-3} to 10^{-5} M.

Comparison between the Structures of Atx1 in Its Reduced Apo and Cu(I) Forms and Its Form in the Presence of Apo-Ccc2a—The solution structure of Cu(I)-^{15} NAtx1 in the presence of apo-Ccc2a at a 1:1 protein ratio (adduct-Cu(I)Atx1 hereafter) has been compared with the mean energy-minimized structures of Cu(I)- and apo-Atx1. In Fig. 7, the three structures are superimposed. The r.m.s. deviation values between Cu(I)- and apo-Atx1 are 1.53 and 1.96 Å for backbone and heavy atoms, respectively. The r.m.s. deviation values between Cu(I)-Atx1 and adduct-Cu(I)Atx1 are 1.27 and 1.74 Å for backbone and heavy atoms, respectively, while the values between apo-Atx1 and adduct-Cu(I)Atx1 are 1.45 and 1.90 Å. As expected, the overall folding of adduct-Cu(I)Atx1 is essentially identical to that of the copper-bound and apo forms. Regions where the r.m.s. deviation between any pair of average structures is larger than the sum of r.m.s. deviation of each family are characterized by real conformational differences. In Fig. 8, the r.m.s. deviation between the average structures of a protein pair, which accounts for structural variations, is compared (as the difference value) with the sum of the r.m.s. deviation values within the families of the two proteins (*i.e.* their structure precision). These differences are estimated for the apo-Atx1/adduct-Cu(I)Atx1 (*solid line*) and Cu(I)-Atx1/adduct-Cu(I)Atx1

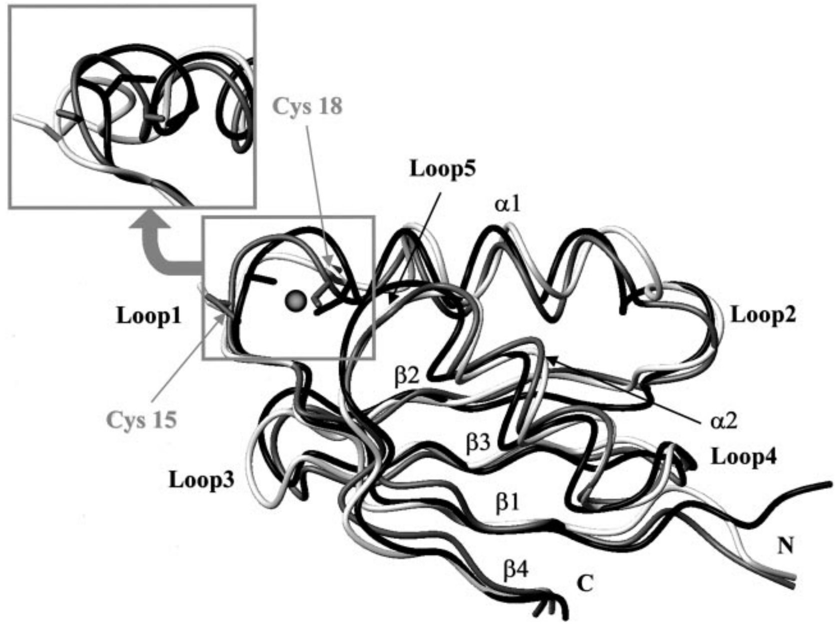

FIG. 7. **Backbone drawing of Cu(I)-Atx1 (*black*), apo-Atx1 (*white*), and Atx1 in the adduct 1:1, Cu(I)-[15]NAtx1/apo-Ccc2a (*gray*).** The copper ion is colored in *black*. Cys[15], Cys[18], and the secondary structure elements are indicated. The *inset* shows an enlarged view of loop 1.

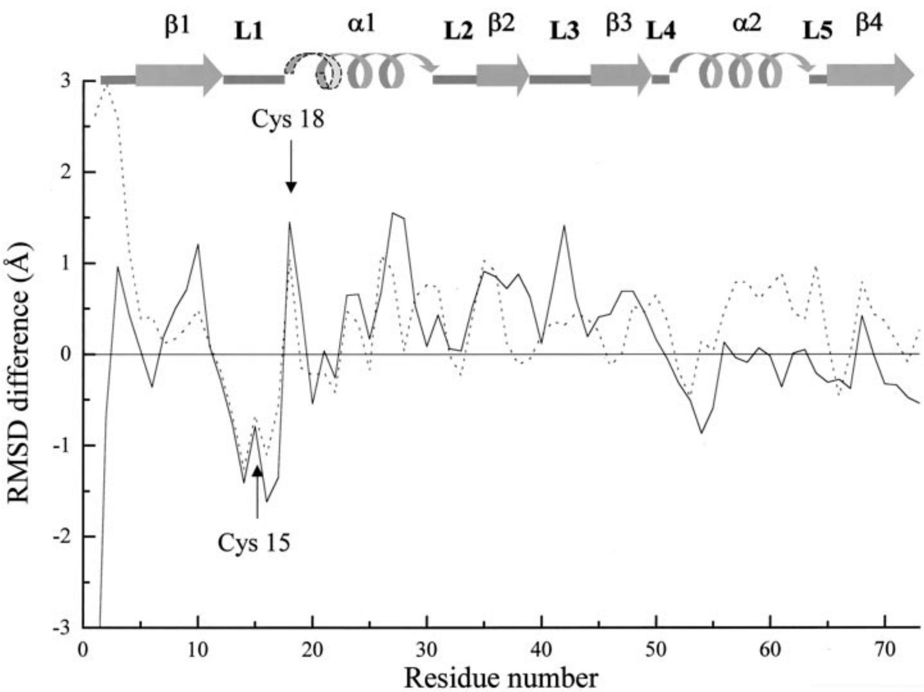

FIG. 8. **Difference between the backbone r.m.s. deviation per residue for the average structures of a protein pair and the sum of the r.m.s. deviation values to the average structure of the two corresponding families (apo-Atx1/adduct-Cu(I)Atx1 (*solid line*) and Cu(I)-Atx1/adduct-Cu(I)Atx1 (*dashed line*)).**

(*dashed line*) pairs. If the structural variations are larger than the sum of the r.m.s. deviation (*i.e.* the difference reported in Fig. 8 is larger than 0), then the structural variations are outside the indetermination of the structures and therefore meaningful. Thus, values varying from 0 result from differences outside the indetermination of the structures. While changes for Cys[15] are not significant, Cys[18] clearly has a different average conformation in the adduct-Cu(I)Atx1 with respect to both Cu(I)- and apo-Atx1. In fact, the superposition of Fig. 7 indicates that the conformation of loop 1 and the N-terminal part of helix α_1 in the adduct-Cu(I)Atx1 is intermediate between that of Cu(I)- and apo-Atx1. In Cu(I)-Atx1, loop 1 (containing Cys[15]) and the beginning of helix α_1 (containing Cys_{18}) are well defined. In apo-Atx1, loop 1 is less well defined, and the last turn of helix α_1 is missing (23). In the present average structure, the metal binding region is again different and intermediate between Cu(I)-loaded and apo-Atx1 structures. Finally, there are differences in the strand β_2 and loop 3 between the isolated proteins with respect to the adduct-Cu(I)Atx1, due to translations of these structural elements. Differences in loop 5 and helix α_2 are only found for the adduct-Cu(I)Atx1 when compared with Cu(I)-Atx1, while the r.m.s. deviation values drop in the comparison with apo-Atx1. In particular, helix α_2 and loop 5 of apo and adduct-Cu(I)Atx1 move away from the copper binding region with respect to Cu(I)-Atx1. The structure of Cu(I)-[15]NAtx1 in the presence of apo-Ccc2a therefore represents an average intermediate between the free Cu(I)-bound and apo states of Atx1.

A Model of the Atx1-Ccc2 Complex—Residues of Cu(I)-[15]NAtx1 that experienced large shifts during the titration are depicted in Fig. 9 (*top panel*). The residues of Cu(I)-[15]NAtx1 most affected by the interaction with apo-Ccc2a are the two cysteines that bind copper and the amino acids in the copper binding region. In Cu(I)-[15]NAtx1, the positively charged ly-

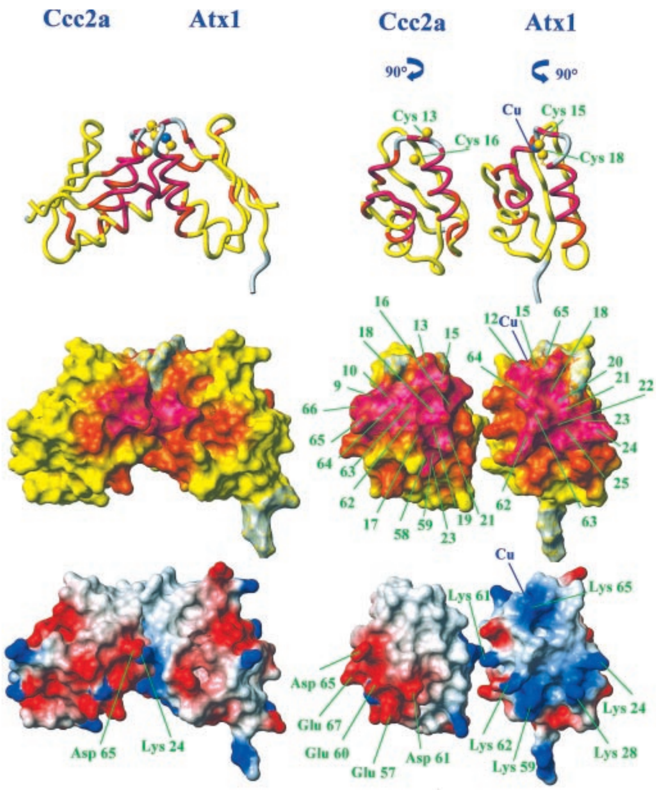

FIG. 9. **Schematic drawing of the Ccc2a/Atx1 adduct model based on the crystal structure of Cu(I)-Hah1 (30).** The *color code* is as follows: *magenta*, $\Delta_{avg}(HN) > 0.1$ ppm; *orange*, $0.04 < \Delta_{avg}(HN) < 0.1$ ppm; *yellow*, $\Delta_{avg}(HN) < 0.04$ ppm; *white*, not observed. The residues are indicated that experience large shift change ($\Delta_{avg}(HN) > 0.1$ ppm). Chemical shift differences $\Delta_{avg}(HN)$ are reported in Figs. 5 and 6 for Atx1 and Ccc2a, respectively. An electrostatic surface representation of the Cu(I) form of Atx1 and apo-Ccc2a is shown in the *lower panels*. The positively charge, negatively charged, and neutral amino acids are represented in *blue*, *red*, and *white*, respectively. The views on the *right side* are the molecules rotated by 90° to allow for viewing of the interaction surfaces.

sines 24, 28, 62, and 65 showed sizeable shifts corresponding to a different environment in solution after the addition of apo-Ccc2a. Negative residues on the Ccc2a interaction surface could interact with the conserved positive face of Atx1. Mutational studies on Atx1 reveal that altering lysines 24 and 28 to Glu dramatically reduces the activity of Atx1, while mutations of lysines 61 and 62 reduce function to a lesser extent (29). Lys^{65} is always conserved in Atx1 homolog sequences from various organisms, and its Nζ is found close to copper (5.0 ± 1.0 Å) in the solution structure of yeast Cu(I)-Atx1 (23) and to the mercury (5.2 Å) in the x-ray structure of Hg(II)-Atx1 (26). Surprisingly, variants K65A and K65F exhibit a nearly wild-type level of activity, while K65E abrogates the activity of Atx1 (29).

The metal binding region of Cu(I)-^{15}NCcc2a is structurally very similar to that of the apo form (24). The release of copper does not cause large structural changes in Ccc2a, suggesting that, unlike apo-Atx1, the metal site in apo-Ccc2a is preorganized to some extent (24). Fig. 9 also shows residues of Cu(I)-^{15}NCcc2a that experienced a large shift or broadening after the addition of apo-Atx1. These are probably involved in the protein interaction. The most affected residues of Cu(I)-^{15}NCcc2a, besides the two copper binding cysteines, were Thr^{17}, Thr^{19}, Asn^{21}, Gln^{23}, Ile^{58}, Cys^{62}, Gly^{63}, Phe^{64}, and Asp^{65}. These residues are located in helix α_1, helix α_2, loop 5, and sheet β_4. Six of these residues are hydrogen bond donors and acceptors, and the hydrophobic side chain of Ile^{58} is solvent-exposed. Phe^{64} is in direct van der Waals contact with the ligating residue Cys^{16}.

Any model of the adduct must be consistent with the observation that any equilibrium among the species present in solution is in fast exchange, since only one signal per nucleus was observed in either case. Furthermore, it should be kept in mind that the same average species is obtained when mixing the two proteins, regardless of which is the protein carrying the copper ion. From what is known about the system, copper will be distributed over the two proteins at the end of the titration. There is 1 mol of metal ion/2 mol of proteins, the affinity for copper of the two proteins is comparable, and adduct formation is far from complete. Finally, it should be noted that copper(I) may expand its coordination number either with exogenous ligands, like a buffer thiol, or may bind two protein molecules, as in the case of the crystal structure of human homodimer Atx1 (Hah1) in the presence of Cu(I), Hg(II), and Cd(II) (30). Hah1 exhibits a β-α-β-β-α-β fold similar to those of yeast Atx1 and Ccc2a. From sequence alignment, the residue identity of Hah1 with Atx1 and Ccc2a is 38 and 25%, respectively. The crystal structure of Cu(I)$(Hah1)_2$ reveals a copper ion coordinated by cysteine residues from two adjacent Hah1 molecules. Nonetheless, the indetermination inherent in the refined distance constraints is large enough that we cannot assign the location of Cu(I) to one site or the other in the adducts of Atx1 and Ccc2a. In fact, the metal may be in rapid exchange between the Atx1 and Ccc2 sites, relative to the NMR time scale. A copper coordination number of four in the adduct is hardly consistent with fast exchange. Indeed, in this case, copper is expected to exchange slowly between free Cu(I) and the bound Atx1 or Ccc2a forms because of chelation. We may propose a coordination number of three as an intermediate that would allow one protein to leave as its apo form. The fast exchange in a complex system like the present one is consistent with the proposal that copper exchange is kinetically favored via juxtaposition of the copper donor and acceptor metal-binding domains. This "three-coordinative" mechanism is also supported by NMR studies performed on Cu(I) and Hg(II) glutathione complexes (72, 73). Indeed, these studies showed that the metal is rapidly exchanged among thiol ligands via transient formation of an Hg(II)-$(thiol)_3$ complex and that the high thermodynamic stability of Cu(I)–S bonds in the complexes is coupled with their kinetic lability. The different overall charge between the two proteins favors protein-protein interactions and the metal ion templates a facile exchange via a series of two- and three-coordinate intermediates (12). The chemical shift perturbation analysis supports this model and further demonstrates significant protein-protein interaction along a docking interface that includes the MTC*XX*C metal-binding motif.

On the basis of chemical shift mapping and the x-ray structure of Cu(I)$(Hah1)_2$ (30), a model for the Atx1-Ccc2a interaction was postulated. Residues experiencing chemical shift perturbation were placed at the interface of the two molecules. Then the relative orientation of the two molecules was optimized to maximize the interaction surface and contacts between oppositely charged residues (Fig. 9). In this model, helix α_1 of one protein is in contact with loop 5 of the partner, but the two helices α_1 are tilted of about 45° to allow a close contact between the two metal binding regions of the two proteins. From the structure of adduct-Cu(I)Atx1, it appears that the conserved Lys^{65} may be involved in the stabilization of the copper binding loop of Atx1 instead of in an electrostatic interaction with Ccc2a. In fact, the positive charge of the side chain of Lys^{65}, located in loop 5 of Atx1, stabilizes the negative charge of the Cu(I) bisthiolate center, and its approach toward the copper site is favored by a translation of helix α_2 and loop 5 upon copper binding (23). This explains the fact that when

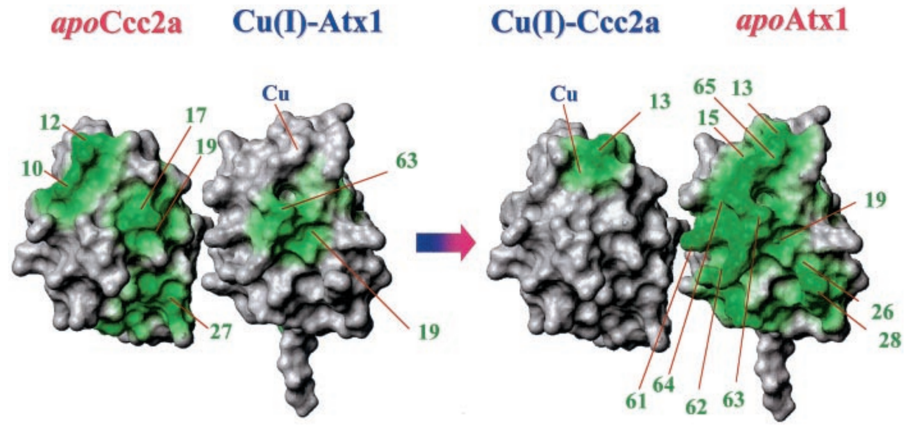

FIG. 10. **Residues experiencing conformational exchange processes in the apo and Cu(I)-loaded forms of Atx1 and Ccc2a are mapped in *green* on the interaction surface of the two proteins.** The structures are oriented as in Fig. 9.

Lys[65] is mutated to neutral residues, the copper delivery to Ccc2 is not affected. On the other hand, an electrostatic interaction is possible between Asp[65] of Ccc2a and Lys[24] of Atx1, which are both conserved in homologous eukaryote sequences. Other side chains whose ^{15}N and ^{1}H shifts are largely affected by the addition of the partner protein are those of Gln[23] of Cu(I)-^{15}NCcc2a and Gln[43] of Cu(I)-^{15}NAtx1. Based on our model, one ϵ-NH of Gln[23] may form a hydrogen bond with the carboxyl group of Lys[61] of Atx1. Gln[23] of Ccc2a is also close to the side chain of the conserved Lys[62] of Atx1. As already pointed out, these two Lys residues of Atx1 experience large shift changes. On the other hand, the side chain of Gln[43] of Atx1 is not close to any residue of Ccc2a in the model of the adduct. However, besides direct protein-protein interactions, secondary effects on the shifts may be at work. In fact, ϵ-NH of Gln[43] (loop 3) forms a hydrogen bond with the carboxyl group of Met[13] (loop 1) in the structure of Cu(I)-Atx1 (23) as well as in the adduct-Cu(I)Atx1. Thus, conformational changes detected in loop 1 translate into shift changes in loop 3.

Mechanistic Implications—Copper transfer is postulated to occur by the following mechanism (12, 74). In a first step, Cu(I)-Atx1 docks transiently in a specific orientation with apo-Ccc2a to poise the system for copper transfer. In a following step, the copper rapidly partitions between the two sites within the protein-protein complex via a series of bridged intermediates, and, finally, the complex dissociates to provide apo-Atx1 and Cu(I)-Ccc2a.

In our titration studies, Cu(I)-^{15}NAtx1 accesses at least two different conformational states as a function of added apo-Ccc2, and this is reflected in the observation of shift changes of Cu(I)-^{15}NAtx1 in the absence and in the presence of apo-Ccc2a. The formation of a bridged intermediate is assumed in the published mechanism of copper transfer (12). The adduct-Cu(I)Atx1 structure represents an intermediate step in the copper trafficking for the following reasons: (i) the shifts of this form of Atx1 are apparent after the first addition of apo-Ccc2a to Cu(I)-^{15}NAtx1; (ii) the increased rotational correlation time of this form must be due to the formation of a higher molecular weight species (*i.e.* the adduct of Atx1 and Ccc2a); and (iii) those residues most altered in the complexed form are located in the metal binding region itself and areas adjacent in space, including loop 5. Structural precedence for a bridged intermediate, albeit a homodimer, is found in the crystal structure of Cu(I)-Hah1. In this structure, copper is coordinated by two Cys from one Hah1 molecule and the N-terminal Cys in the M*X*C*XX*C motif of a second molecule plus a fourth sulfur at a longer distance (30). The changes in signal detectability for Cys[18] and Cys[15] in apo-Atx1 and Cu(I)-Atx1 (23) are in agreement with the mechanism of copper transfer (28, 74). Indeed, it can be suggested that Cys[15] of Cu(I)-Atx1, which is the most exposed, interacts with apo-Ccc2a when the protein-protein complex is formed, while Cys[18] is detached at first from copper coordination in Atx1, thus becoming more mobile. Moreover, Cys[18] experiences a conformational change in the structure of adduct-Cu(I)Atx1 compared with both Cu(I) and apo-Atx1 (see Figs. 7 and 8). A similar trigger mechanism upon metal binding has been suggested for the mercuric ion-binding protein MerP (75). In MerP, it has been proposed that Hg(II) initially binds the solvent-exposed Cys[14] and then attracts the negatively charged thiol group of the Cys[17] from its inaccessible position, thus causing the structural change (75, 76).

Mobility measurements for apo-^{15}NAtx1 and Cu(I)-^{15}NAtx1 also provide some information about the different forms of Atx1 as a function of copper transfer and release. An increased number of residues experiencing conformational exchange in the millisecond to microsecond time scale was found in apo- compared with Cu(I)-^{15}NAtx1. Evidence of additional motions on a slow time scale has also been observed for reduced apo-MerP with respect to the metal-loaded state, suggesting that, in this case also, the metal binding site can "flap" or "breathe" slowly without a bound metal (76).

In apo-Atx1, mobile residues in the millisecond to microsecond time range are those located in loops 1 and 5 and helices α_1 and α_2. This region corresponds to those residues that change the most in chemical shift perturbation analysis and that are modeled to the interaction interface of the docked complex (Fig. 10). Thus, mobility in this region of apo-Atx1 could favor complex dissociation of the two proteins after copper release. On the other hand, the difference in the dynamic behavior observed in the Cu(I)-loaded and apo-Ccc2a is less pronounced, according to the fact that the two forms of the protein are structurally very similar, as also found for a domain of the Ccc2 human homologue, Menkes protein (77). The copper chaperones, from yeast to humans, have a conserved Lys in loop 5 (Lys[65] in Atx1), very close to the copper site. Interestingly, this region (residues 61–65) becomes more mobile in the millisecond to microsecond time range when copper is released. This does not occur in apo-Ccc2a, where Lys is replaced by a hydrophobic residue, Phe[64], which is conserved among eukaryotic ATPases. This difference between Ccc2a and Atx1 may be related to the different roles of these two proteins in the copper trafficking pathway. The ATPase has a stable metal binding region preorganized for copper uptake, while the observed flexibility of apo-Atx1 may provide a trigger for metal release and allow the chaperone to adapt to its two partners, *i.e.* downstream of CTR1 and upstream of Ccc2.

Acknowledgment—We thank Prof. Anthony G. Wedd for careful reading of the manuscript and for extensive discussion.

REFERENCES

1. Askwith, C., and Kaplan, J. (1998) *Trends Biochem. Sci.* **23,** 135–138
2. Kaplan, J., and O'Halloran, T. V. (1996) *Science* **271,** 1510–1512
3. Dancis, A., Yuan, D. S., Haile, D., Askwith, C., Elde, D., Moehle, C., Kaplan, J., and Klausner, R. D. (1994) *Cell* **76,** 393–402
4. Dancis, A., Haile, D., Yuan, D. S., and Klausner, R. D. (1994) *J. Biol. Chem.* **269,** 25660–25667
5. Zhou, B., and Gitschier, J. (1997) *Proc. Natl. Acad. Sci. U. S. A.* **94,** 7481–7486
6. Pena, M. M. O., Lee, J., and Thiele, D. J. (1999) *J. Nutr.* **129,** 1251–1260
7. Fu, D., Beeler, T. J., and Dunn, T. M. (1995) *Yeast* **11,** 283–292
8. Yuan, D. S., Stearman, R., Dancis, A., Dunn, T., Beeler, T., and Klausner, R. D. (1995) *Proc. Natl. Acad. Sci. U. S. A.* **92,** 2632–2636
9. Yuan, D. S., Dancis, A., and Klausner, R. D. (1997) *J. Biol. Chem.* **272,** 25787–25793
10. Askwith, C., Eide, D., Van Ho, A., Bernard, P. S., Li, L., Davis-Kaplan, S., Sipe, D. M., and Kaplan, J. (1994) *Cell* **76,** 403–410
11. Lin, S. J., Pufahl, R., Dancis, A., O'Halloran, T. V., and Culotta, V. C. (1997) *J. Biol. Chem.* **272,** 9215–9220
12. Pufahl, R., Singer, C. P., Peariso, K. L., Lin, S.-J., Schmidt, P. J., Fahrni, C. J., Cizewski Culotta, V., Penner-Hahn, J. E., and O'Halloran, T. V. (1997) *Science* **278,** 853–856
13. Klomp, L. W., Lin, S. J., Yuan, D., Klausner, R. D., Culotta, V. C., and Gitlin, J. D. (1997) *J. Biol. Chem.* **272,** 9221–9226
14. Vulpe, C. D., Levinson, B., Whitney, S., Packman, S., and Gitschier, J. (1993) *Nat. Genet.* **3,** 7–13
15. Bull, P. C., Thomas, G. R., Rommens, J. M., Forbes, J. R., and Cox, D. W. (1993) *Nat. Genet.* **5,** 327–337
16. Mercer, J. F., Livingstone, J., Hall, B., Paynter, J. A., Begy, C., Chandrasekharappa, S., Lockhart, P., Grimes, A., Bhave, M., Siemieniak, D., and Glover, T. W. (1993) *Nat. Genet.* **3,** 20–25
17. Chelly, J., Tumer, Z., Tonnesen, T., Petterson, A., Ishikawa-Brush, Y., Tommerup, N., Monaco, A. P., and Horn, N. (1993) *Nat. Genet.* **3,** 14–19
18. Vulpe, C. D., Kuo, Y. M., Murphy, T. L., Cowley, L., Askwith, C., Libina, N., Gitschier, J., and Anderson, G. J. (1999) *Nat. Genet.* **21,** 195–199
19. Hung, I. H., Casareno, R. L., Labesse, G., Mathews, F. S., and Gitlin, J. D. (1998) *J. Biol. Chem.* **273,** 1749–1754
20. Hung, I. H., Suzuki, M., Yamaguchi, Y., Yuan, D. S., Klausner, R. D., and Gitlin, J. D. (1997) *J. Biol. Chem.* **272,** 21461–21466
21. Forbes, J. R., Hsi, G., and Cox, D. W. (1999) *J. Biol. Chem.* **274,** 12408–12413
22. Larin, D., Mekios, C., Das, K., Ross, B., Yang, A. S., and Gilliam, C. T. (1999) *J. Biol. Chem.* **274,** 28497–28504
23. Arnesano, F., Banci, L., Bertini, I., Huffman, D. L., and O'Halloran, T. V. (2001) *Biochemistry* **40,** 1528–1539
24. Banci, L., Bertini, I., Ciofi-Baffoni, S., Huffman, D. L., and O'Halloran, T. V. (2001) *J. Biol. Chem.* **276,** 8415–8426
25. Gitschier, J., Moffat, B., Reilly, D., Wood, W. I., and Fairbrother, W. J. (1998) *Nat. Struct. Biol.* **5,** 47–54
26. Rosenzweig, A. C., Huffman, D. L., Hou, M. Y., Wernimont, A. K., Pufahl, R. A., and O'Halloran, T. V. (1999) *Structure* **7,** 605–617
27. Hubbard, T. J. P., Murzin, A. G., Brenner, S. E., and Chothia, C. (1997) *Nucleic Acids Res.* **25,** 236–239
28. Huffman, D. L., and O'Halloran, T. V. (2000) *J. Biol. Chem.* **275,** 18611–18614
29. Portnoy, M. E., Rosenzweig, A. C., Rae, T., Huffman, D. L., O'Halloran, T. V., and Cizewski Culotta, V. (1999) *J. Biol. Chem.* **274,** 15041–15045
30. Wernimont, A. K., Huffman, D. L., Lamb, A. L., O'Halloran, T. V., and Rosenzweig, A. C. (2000) *Nat. Struct. Biol.* **7,** 766–771
31. Bradford, M. (1976) *Anal. Biochem.* **72,** 248–254
32. Riddles, P. W., Blakeley, R. L., and Zerner, B. (1983) *Methods Enzymol.* **91,** 49–60
33. Palmer, A. G., III, Cavanagh, J., Wright, P. E., and Rance, M. (1991) *J. Magn. Reson.* **93,** 151–170
34. Kay, L. E., Keifer, P., and Saarinen, T. (1992) *J. Am. Chem. Soc.* **114,** 10663–10665
35. Schleucher, J., Schwendinger, M., Sattler, M., Schmidt, P., Schedletzky, O., Glaser, S. J., Sorensen, O. W., and Griesinger, C. (1994) *J. Biomol. NMR* **4,** 301–306
36. Bax, A., and Davis, D. G. (1985) *J. Magn. Reson.* **63,** 207–213
37. Griesinger, C., Otting, G., Wüthrich, K., and Ernst, R. R. (1988) *J. Am. Chem. Soc.* **110,** 7870–7872
38. Macura, S., Wüthrich, K., and Ernst, R. R. (1982) *J. Magn. Reson.* **47,** 351–357
39. Davis, L. A., Keller, J., Laue, E. D., and Moskau, D. (1992) *J. Magn. Reson.* **98,** 207–216
40. Kay, L. E., Nicholson, L. K., Delaglio, F., Bax, A., and Torchia, D. A. (1992) *J. Magn. Reson.* **97,** 359–375
41. Peng, J. W., and Wagner, G. (1994) *Methods Enzymol.* **239,** 563–596
42. Grzesiek, S., and Bax, A. (1993) *J. Am. Chem. Soc.* **115,** 12593–12594
43. Marion, D., and Wüthrich, K. (1983) *Biochem. Biophys. Res. Commun.* **113,** 967–974
44. Piotto, M., Saudek, V., and Sklenar, V. (1992) *J. Biomol. NMR* **2,** 661–666
45. Eccles, C., Güntert, P., Billeter, M., and Wüthrich, K. (1991) *J. Biomol. NMR* **1,** 111–130
46. Marquardt, D. W. (1963) *J. Soc. Ind. Appl. Math.* **11,** 431–441
47. Press, W. H., Flannery, B. P., Teukolsky, S. A., and Vetterling, W. T. (1988) *Numerical Recipes in C: The Art of Scientific Computing*, Cambridge University Press, New York
48. Palmer, A. G., III, Rance, M., and Wright, P. E. (1991) *J. Am. Chem. Soc.* **113,** 4371–4380
49. Peng, J. W., and Wagner, G. (1992) *Biochemistry* **31,** 8571–8586
50. Zinn-Justin, S., Berthault, P., Guenneugues, M., and Desvaux, H. (1997) *J. Biomol. NMR* **10,** 363–372
51. Mandel, M. A., Akke, M., and Palmer, A. G., III (1995) *J. Mol. Biol.* **246,** 144–163
52. Lipari, G., and Szabo, A. (1982) *J. Am. Chem. Soc.* **104,** 4546–4559
53. Abragam, A. (1961) *The Principles of Nuclear Magnetism*, Oxford University Press, Oxford
54. Brüschweiler, R., Liao, X., and Wright, P. E. (1995) *Science* **268,** 886–889
55. Lee, L. K., Rance, M., Chazin, W. J., and Palmer, A. G., III (1997) *J. Biomol. NMR* **9,** 287–298
56. Schurr, J. M., Babcock, H. P., and Fujimoto, B. S. (1994) *J. Magn. Reson. Ser. B* **105,** 211–224
57. Tjandra, N., Wingfield, P., Stahl, S., and Bax, A. (1996) *J. Biomol. NMR* **8,** 273–284
58. Luginbuhl, P., Pervushin, K. V., Iwai, H., and Wüthrich, K. (1997) *Biochemistry* **36,** 7305–7312
59. Orekhov, V. Y., Pervushin, K. V., and Arseniev, A. S. (1994) *Eur. J. Biochem.* **219,** 887–896
60. Bloom, M., Reeves, L. W., and Wells, E. J. (1965) *J. Chem. Phys.* **42,** 1615–1624
61. Güntert, P., Braun, W., and Wüthrich, K. (1991) *J. Mol. Biol.* **217,** 517–530
62. Güntert, P., Mumenthaler, C., and Wüthrich, K. (1997) *J. Mol. Biol.* **273,** 283–298
63. Borgias, B., Thomas, P. D., and James, T. L. (1989) *Complete Relaxation Matrix Analysis (CORMA)*, University of California, San Francisco
64. Laskowski, R. A., MacArthur, M. W., Moss, D. S., and Thornton, J. M. (1993) *J. Appl. Crystallogr.* **26,** 283–291
65. Laskowski, R. A., Rullmann, J. A. C., MacArthur, M. W., Kaptein, R., and Thornton, J. M. (1996) *J. Biomol. NMR* **8,** 477–486
66. Kay, L. E., Torchia, D. A., and Bax, A. (1989) *Biochemistry* **28,** 8972–8979
67. Tjandra, N., Feller, S. E., Pastor, R. W., and Bax, A. (1995) *J. Am. Chem. Soc.* **117,** 12562–12566
68. Cantor, R. C., and Schimmel, P. R. (1980) *Biophysical Chemistry*, Freeman, W. H., San Francisco
69. Wimmer, R., Herrmann, T., Solioz, M., and Wüthrich, K. (1999) *J. Biol. Chem.* **274,** 22597–22603
70. Lian, L. Y., and Roberts, G. C. K. (1993) *NMR of Macromolecules: A Practical Approach*, Oxford University Press, Oxford
71. Garrett, D. S., Seok, Y. J., Liao, D. I., Peterkofsky, A., Gronenborn, A. M., and Clore, G. M. (1997) *Biochemistry* **36,** 2517–2530
72. Corazza, A., Harvey, I., and Sadler, P. J. (1996) *Eur. J. Biochem.* **236,** 697–705
73. Cheesman, B. V., Arnold, A. P., and Rubenstein, D. L. (1988) *J. Am. Chem. Soc.* **110,** 6359–6364
74. Huffman, D. L., O'Hallorah, T. V. (2001) *Ann. Rev. Biochem.* **70,** 677–701
75. Powlowski, J., and Sahlman, L. (1999) *J. Biol. Chem.* **274,** 33320–33326
76. Steele, R. A., and Opella, S. J. (1997) *Biochemistry* **36,** 6885–6895
77. Qin, J., La Mar, G. N., Cutruzzula, F., Allocatelli, C. T., Brancaccio, A., and Brunori, M. (1993) *Biophys. J.* **65,** 2178–2190

Characterization of the Binding Interface between the Copper Chaperone Atx1 and the First Cytosolic Domain of Ccc2 ATPase

Fabio Arnesano, Lucia Banci, Ivano Bertini, Francesca Cantini, Simone Ciofi-Baffoni, David L. Huffman and Thomas V. O'Halloran

J. Biol. Chem. 2001, 276:41365-41376.
doi: 10.1074/jbc.M104807200 originally published online August 10, 2001